IEEE/CSC & ESAS SUPERCONDUCTIVITY NEWS FORUM (global edition), October 2015.
Invited poster presentation 3A-LS-O1.7 given at EUCAS 2015; Lyon, France, September 6 – 10, 2015.
A manuscript was submitted to *IEEE Trans. Appl. Supercond.* for possible publication.

Coupled Mechanical and Electrical Modeling of Nb_3Sn Strand Critical Current under Bending

D. Ciazynski, A. Torre, S. Li, and G. Lenoir

***Abstract*—Strain dependence of Nb_3Sn superconducting properties is known to be responsible for the degradation of transport current capability of large steel jacketed cable-in-conduit conductors (CICCs). The mechanical deformations of the strands in the cables due to both cool down after heat treatment and Lorentz force during operation, are the main sources of strand-in-cable critical current degradation. The complete modeling of a CICC relies first on the modeling of the single strand with its superconducting filaments then on the modeling of the strands in the cable. The paper reports on the description of the models and the analyses performed using coupled mechanical and electrical modeling. The key of this modeling lies in its ability to characterize the superconducting properties of the twisted Nb_3Sn filaments inside a locally bent strand from a global mechanical deformation map, taking into account possible current redistribution among filaments all along the strand length. In the same way, strands may experience local critical current degradation in a CICC and current transfer between strands at their contact points must be modeled to predict cable performance. This work can be seen as the first stones of an integrated coupled mechanical-electrical modeling of large CICCs made with strain sensitive strands.**

***Index Terms*—Niobium tin, degradation, bending, modeling, cable-in-conduit, fusion magnets.**

I. Introduction

STRAIN dependence of Nb_3Sn superconducting properties is known to be responsible for the degradation of transport current capability (or temperature margin) of large steel jacketed cable-in-conduit conductors (CICCs) made with about one thousand strands. This phenomenon was particularly observed on the big ITER Nb_3Sn CICCs, either in the model coils or in conductor qualification samples [1], [2] and must be anticipated for still larger current conductors expected in the future fusion reactors. The mechanical deformations of the strands under compression and bending in the cables, due to both cool down after heat treatment and Lorentz force during operation, have been identified as the main sources of strand-in-cable critical current degradation. In order to better understand this phenomenon, a collaborative action has been launched between CEA/IRFM and Ecole CentraleSupélec, ECS/LMSSMat, where CEA takes in charge electrical modeling and measurements whereas ECS is responsible for mechanical modeling and characterizations. The coupling between mechanical and electrical models is made through the build of a strain map in the strand cross-section along each strand which is used as an input to compute the Nb_3Sn critical current density in the electrical model [3].

This work was supported in part by the French Agence Nationale de la Recherche within the Cocascope project.

D. Ciazynski and A. Torre are with the CEA/IRFM, Centre de Cadarache, 13108 Saint-Paul-lez Durance, France (e-mail: daniel.ciazynski@cea.fr and alexandre.torre@cea.fr).

S. Li is with the Ecole Centrale Lyon, 69134 Ecully, France, and was in a short stay at CEA/IRFM (e-mail: shijun.li@ecl13.ec-lyon.fr).

G. Lenoir is with the Ecole CentraleSupélec, MSSMat lab., 92295 Châtenay-Malabry, France (e-mail: gilles.lenoir@centralesupelec.fr).

II. Modeling of a Single Strand under Bending

A. Presentation of the experimental device

Critical current experiments have been carried out at CEA/IRFM to characterize Nb_3Sn strands under bending using VAMAS-like modified mandrels [4]. These mandrels allow periodic strand bending under the centripetal Lorentz force generated during critical current measurements under applied magnetic field. There are two unsupported parts by turn; therefore the strand encounters alternate supported and bending lengths all along its trajectory (see Fig. 1).

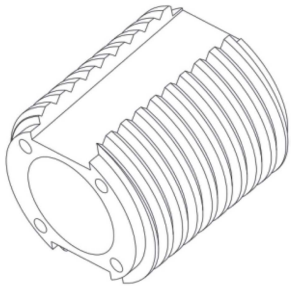

Fig. 1. Drawing of the VAMAS-like mandrel with its 12-mm grooves.

B. Mechanical analysis: strain map

A first mechanical modeling of the experiment was performed by ECS using the Abaqus™ code to analyze a quarter of a turn of the strand on its mandrel with symmetries at both ends. The strand (∅ 0.81 mm) was modeled as a homogeneous medium according to previous analyses [5]. The mechanical computation was performed for a Lorentz force of 4 kN/m, as the maximum value generated during the tests, and for a free length of 12 mm (see Fig. 2).

In a first step, the axial strain map was built from the computed strain along the strand inner and outer radii on the mandrel, assuming a linear variation of strain along the radius in the cross-section and adding afterwards a thermal strain of -0.10% for strand on a Ti mandrel (see Fig. 3).

IEEE/CSC & ESAS SUPERCONDUCTIVITY NEWS FORUM (global edition), October 2015.
Invited poster presentation 3A-LS-O1.7 given at EUCAS 2015; Lyon, France, September 6 – 10, 2015.
A manuscript was submitted to *IEEE Trans. Appl. Supercond.* for possible publication.

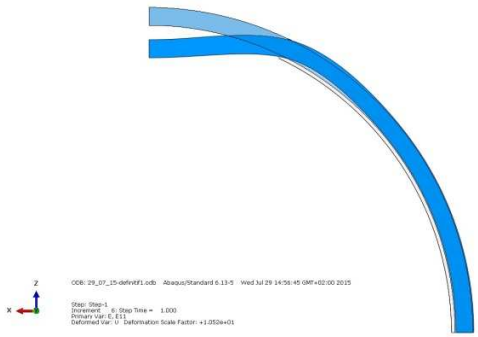

Fig. 2. Deformation (×10) of strand under maximum Lorentz force.

Note that the radius of the filamentary area in the strand is 0.35 mm. As shown in Figs. 2 and 3 the experimental strand deformation is far from being a pure beam bending. From this map, it is then possible to compute the strain ε in any Nb_3Sn filament at any location.

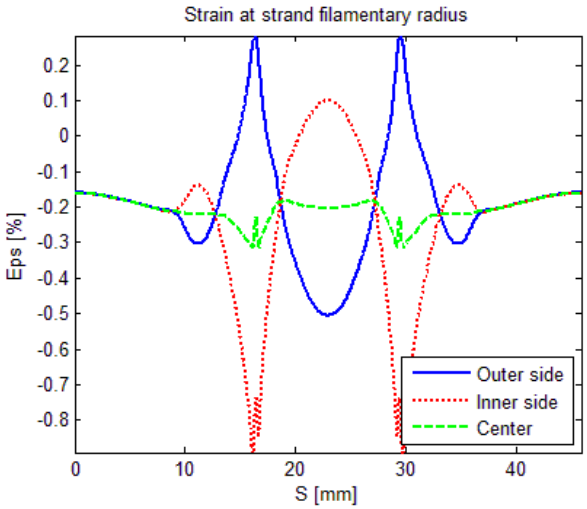

Fig. 3. Axial strain along strand over a half-turn at strand center and on filamentary area extreme radii. Unsupported 12 mm length is at middle.

C. *Electrical modeling*

In a second step, a simplified 7 (six twisted around one) filament bundles model was built in the CEA CARMEN code to be able to compute current and electric field along filaments (see Fig. 4). A strand length of half a turn was modeled which includes the 12 mm free length at middle and two remaining fully supported lengths in each side as in Fig. 3. Inter-bundle resistances are computed from the transverse resistivity ρ_{tran}. At each strand end the bundles are connected to a common node through high series resistances so as to ensure uniform current distribution at ends. The computation step over the length is 0.2 mm.

The mechanical strain map can be converted to Nb_3Sn filament strain using filament twist pitch (14.6 mm pitch) and initial positions. From this strain profiles and using the non-copper critical current density law $J_C(B,T,\varepsilon)$, the critical current of every bundle can be computed all along its trajectory.

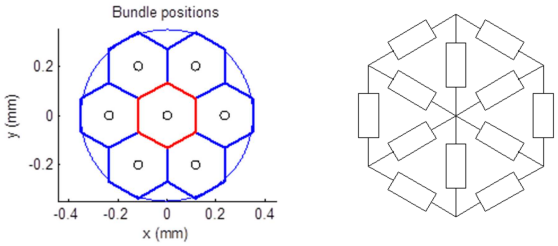

Fig. 4. Strand cross-section with 6+1 bundles (left) and associated transverse (inter-bundle) resistances in any section (right).

The result of this computation for B = 9 T at 4.22 K is given in Fig. 5 where one can see quite low local critical currents due to either high compression or tension. One can also note a kind of 'resonance' between the twist pitch and the high strain areas distance.

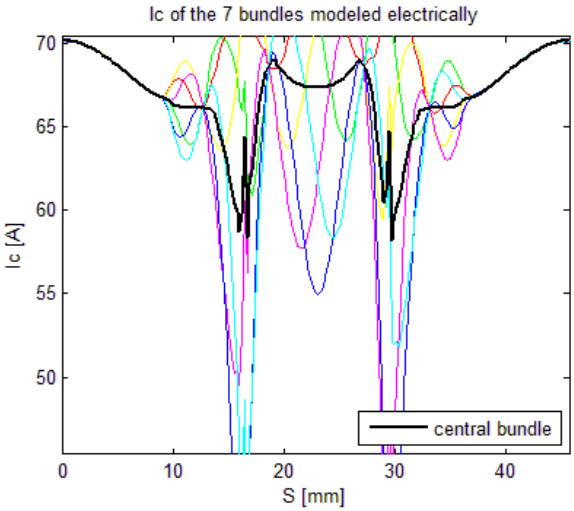

Fig. 5. Critical current along the 7 bundles with central bundle in bold.

D. *Critical current*

The strand critical current is defined as close as possible to the measurement through the mean value of the voltage drops along all bundles over the strand length (except 2 mm removed at each end to eliminate ends effect) and corresponding to an average electric field <E> equal to E_C = 10 µV/m. The n index is set to n = 20 at the filament level and ρ_{tran} = 3.0 10^{-11} Ω.m is used in a first step [3].

Results of the simulation with CARMEN are presented in the forms of bundle currents (Fig. 6) and electric field (Fig. 7).

One can see in Fig. 6 that the bundle currents change over small scales due to high variations of the critical current along bundles (see Fig. 5) and the low transverse resistivity allowing easy current transfer. However, one can also see in Fig. 7 that this transfer is not strong enough to avoid high local electric fields and as a consequence the electric field is significantly peaked (up to 4-5 10^{-4} V/m) at critical locations although its average value over the length remains obviously equal to E_C.

IEEE/CSC & ESAS SUPERCONDUCTIVITY NEWS FORUM (global edition), October 2015.
Invited poster presentation 3A-LS-O1.7 given at EUCAS 2015; Lyon, France, September 6 – 10, 2015.
A manuscript was submitted to *IEEE Trans. Appl. Supercond.* for possible publication.

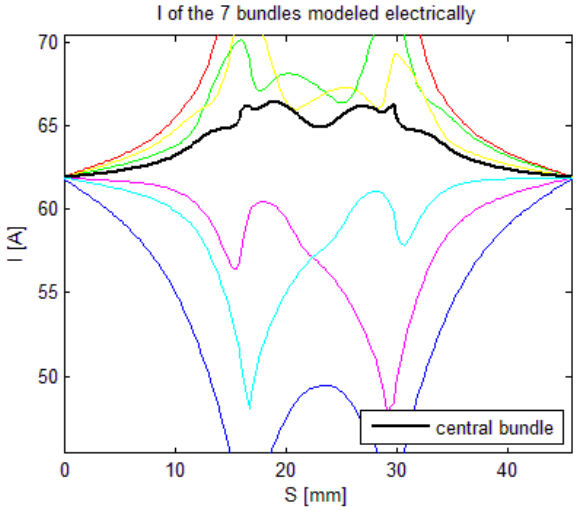

Fig. 6. Bundle currents along the 7 bundles with central bundle in bold.

The maximum strand critical current in each section along the strand length (see Fig. 8) can be fully usable only when the transverse resistivity is low enough, i.e. in the so-called low resistivity limit (LRL). On the other hand, one can also compute by electric field integration the strand critical current in the high resistivity limit (HRL) with insulated bundles [6]. A comparison of the strand critical current given by CARMEN against the LRL and the HRL values is also shown in Fig. 8.

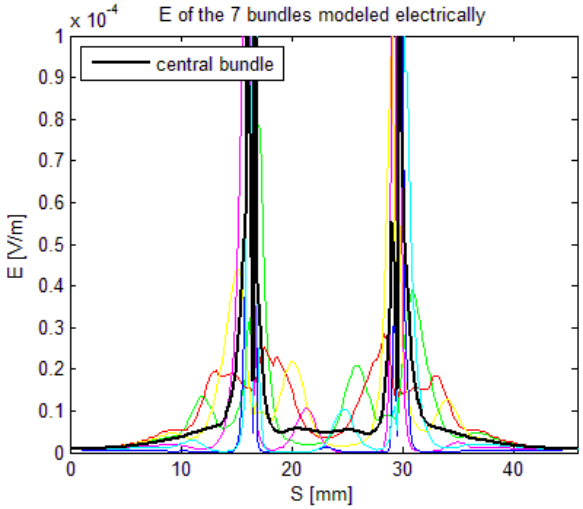

Fig. 7. Electric field along the 7 bundles with central bundle in bold.

The CAMEN result is dependent on the ρ_{tran} value. The lower ρ_{tran} the closer the CARMEN result to the LRL as shown in Table I. However, the simulation result may be lower than the HRL due to the boundary conditions imposed in the CARMEN model where current distribution among bundles is forced to be uniform at strand ends, which is not imposed in the HRL. As a matter of fact, a numerical simulation with very low series resistances at each end has led to I_C = 411 A (instead of 372 A) for ρ_{tran} = 3.0 10^{-9} Ω.m.

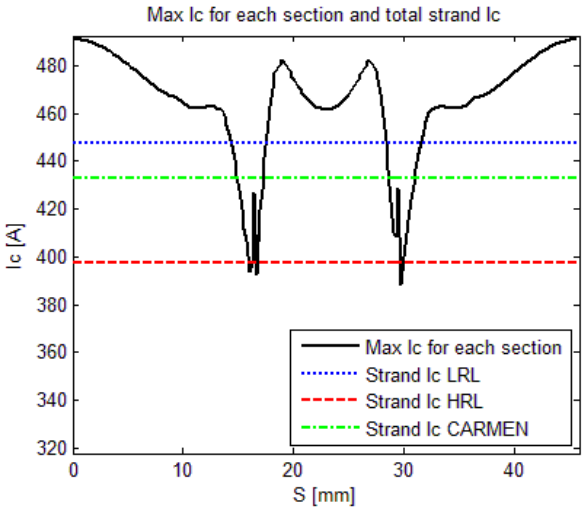

Fig. 8. Max. strand critical current in each section, HRL, LRL, and CARMEN strand critical currents.

The experimental result is I_C = 410 A [4] which is broadly in line with the computations, considering that the $J_C(B,T,\varepsilon)$ is only extrapolated from another similar strand since the law is not fully known for the tested strand, the strain map may be inaccurate due to the use of a homogeneous model and the addition afterwards of the thermal intrinsic strain (= -0.1%).

TABLE I
STRAND CRITICAL CURRENT I_C AS A FUNCTION OF ρ_{tran}

ρ_{tran} (Ω.m)	I_C (A)
∞ (HRL)	398
3.0 10^{-9}	372
3.0 10^{-10}	419
3.0 10^{-11}	432
0 (LRL)	448

III. CURRENT TRANSFER IN A TWO-STRAND CABLE

In a CICC, in addition to a compressive axial strain, every strand experiences local bending along its trajectory, depending on contacts and unsupported lengths [3]. Overstrain tends to decrease local critical current (see Fig. 8) and so to push current transfer between strands. However, in this case the current can transfer between strands only at the contact points and the current always needs to flow through the Nb_3Sn filaments, so this current transfer actually involves current transfer between filaments.

A. Simple Electrical Modeling

A simple two-strand cable electrical model was built in CARMEN to study inter-strand current transfer. The model makes use of the previous 7-bundle strand model along a 60 mm length and assumes 3 contact points between external bundles of each strand at locations s = 20, 30, and 40 mm. There are only two bundles (one per strand) connected through a contact resistance and they are different at each contact. The two strands are connected in parallel using series resistances at each bundle end as previously.

In addition, the problem has been further simplified by considering a local degradation of the critical current of all the

bundles in each strand between contact points (see Fig. 9). Namely, *Ic_high* = 30 A and *Ic_low* = 24 A per bundle.

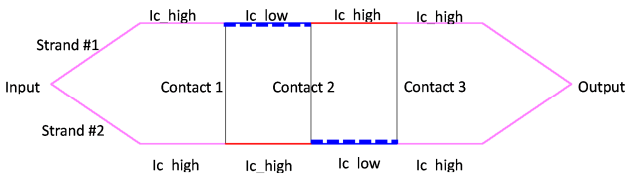

Fig. 9. Scheme of a two-strand cable with 3 contact points.

The computation step over the length is 1 mm, therefore implicitly the contacts spread over 1 mm. The critical current of the cable is computed through the voltage drop from s = 20 to 40 mm so as to mitigate ends effects.

B. Results of simulations

The results of a simulation with a contact resistance equal to the inter-bundle resistance R_{trans} (= 25 nΩ over 1 mm) are presented as a realistic example. The plots of the bundle currents along strand length are shown in Fig. 10, whereas electric field plots are shown in Fig. 11. In these figures, Bjk means bundle #k in strand #j, with k = 1 for central bundle. To help reading these plots, please note that B15-B22, B14-B27, and B17-B24 are involved at contacts 1, 2, and 3, respectively (see also Fig. 9).

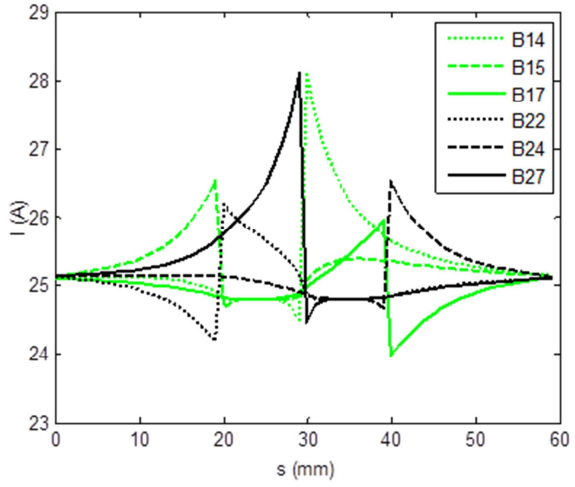

Fig. 10. Bundle currents along cable length.

One can see In Fig. 10 that current transfer between strands acts to decrease the current (and so the electric field) in the weak lengths. Since contacts only involve one bundle per strand, inter-bundle current transfer must be involved prior or after any inter-strand current transfer so as to maximize the contact current. Electric field on the weak bundles is only slightly reduced compared to the value of $2 \times E_C$ needed to get $\langle E \rangle = E_C$ with $E = 0$ along the strong lengths (see Fig. 11).

The effect of the contact resistance R_{cont} on the cable critical current I_C and the 3 contact currents I_{contk} (k = 1 to 3) are reported in Table II. One can see in this table the increases of both I_C and I_{cont} as R_{cont} decreases (associated with the decrease of the currents in the weak parts).

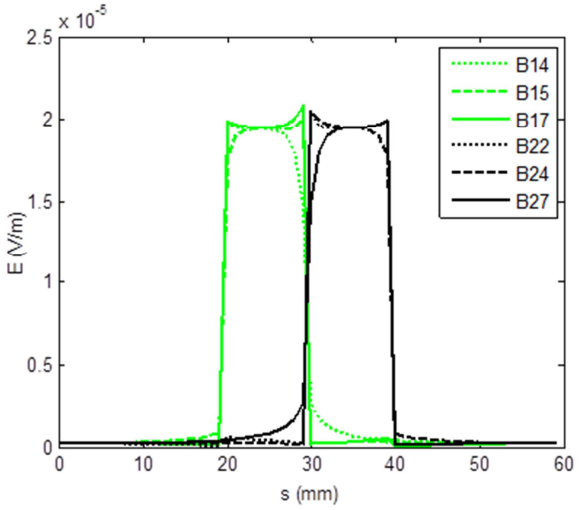

Fig. 11. Electric field in bundles along cable length.

Boundary limits can be computed analytically to be I_{Cmin} = 347.8 A for insulated strands and I_{Cmax} = 378.0 A for equipotential strands (perfect contact). One can see in Table II that both I_C and I_{cont} tend towards limits significantly lower than expected as R_{cont} decreases (see next section).

TABLE II
EFFECT OF CONTACT RESISTANCE ON CRITICAL AND CONTACT CURRENTS

R_{cont}/R_{trans}	I_C (A)	I_{cont1} (A)	I_{cont2} (A)	I_{cont3} (A)
10	348.0	0.2	-0.5	0.2
1	351.9	2.2	-4.5	2.2
0.1	361.2	7.8	-15.9	7.8
0.01	363.9	10.1	-20.2	10.1

C. Simplified two-bundle model

Although the model used in the preceding section was extremely simple, the rather complex form taken by this multiscale problem has become obvious. Therefore, in view of the modelling of a real CICC consisting of tens, see hundreds, of strands, it looks compulsory to consider a kind of "macro-model" for the strand itself, avoiding to deal with the filamentary (even bundle) scale.

Our two-strand cable can then be treated through a simpler two-bundle model, with exactly the same scheme as in Fig. 9. In this case the inter-bundle current transfer in each strand cannot be modeled and the discrepancy with the preceding model becomes clear at low contact resistances (see Table III). However, we have found that this problem may be mitigated by adding to R_{cont} an extra term to consider an effective contact resistance R'_{cont} depending on R_{trans} in the two-bundle model:

$$R'_{cont} = R_{cont} + \alpha * R_{trans}$$

Then, a value α = 0.24 was found optimal for cable critical current with R_{cont} varying over 4 decades (see Table III). Note that the contact current I_{cont2} is then slightly underestimated, the optimal α being rather 0.20 for it.

IEEE/CSC & ESAS SUPERCONDUCTIVITY NEWS FORUM (global edition), October 2015.
Invited poster presentation 3A-LS-O1.7 given at EUCAS 2015; Lyon, France, September 6 – 10, 2015.
A manuscript was submitted to *IEEE Trans. Appl. Supercond.* for possible publication.

TABLE III
EFFECT OF α ON CRITICAL AND CENTRAL CONTACT CURRENT

α	0 (initial)		0.24 (optimal)	
R_{cont}/R_{trans}	I_C (A)	I_{cont2} (A)	I_C (A)	I_{cont2} (A)
10	348.0	-0.5	348.0	-0.5
1	352.4	-5.0	351.6	-4.0
0.1	373.2	-29.5	360.6	-13.7
0.01	377.9	-40.5	363.9	-17.5

IV. CONCLUSIONS

A coupled mechanical and electrical modeling has been set to analyze Nb_3Sn strand bending experiments on dedicated VAMAS-like mandrels. The first results have shown that the strain map was more complex than expected and that high local strain could lead to strong peaking of local electric field pushing significant current transfer between filaments. First results look promising but both mechanical and electrical models still need to be improved in order to better represent the experiment.

First modeling of current transfer between strands in a CICC performed using a two-strand model have shown the complexity of the current transfer at contact points involving inter-filaments current transfer inside connected strands which requires increasing the effective contact resistance when using macro models.

REFERENCES

[1] N. Mitchell, “Summary, assessment and implications of the ITER model coil test results,” *Fus. Eng. and Design*, vol. 66–68, 2003, pp. 971–993.
[2] D. Ciazynski, “Review of Nb_3Sn conductors for ITER,” *Fus. Eng. and Design*, vol. 82, 2007, pp. 488–97.
[3] A. Torre, H. Bajas, and D. Ciazynski, “Mechanical and Electrical Modeling of Strands in Two ITER CS Cable Designs,” *IEEE Trans. Appl. Supercond.*, vol. 24, no. 3, Jun. 2014, Art. ID. 8401105.
[4] A. Torre et al., “A New Experimental Set-Up to Measure Critical Current in Superconducting Strands Under Periodic Bending,” *IEEE Trans. Appl. Supercond.*, vol. 25, no. 3, Jun. 2015, Art. ID. 9001005.
[5] H. Bajas, “Numerical simulation of the mechanical behavior of the ITER cable-in-conduit conductors,” Ph.D. dissertation, Chapt. III, Ecole Centrale Paris, Châtenay-Malabry, France, Mar. 14, 2011.
[6] D. Ciazynski and A. Torre, "Analytical formulae for computing the critical current of an Nb_3Sn strand under bending," *Supercond. Sci. Technol.*, vol. 23, Issue 12, 2010, pp. 125005.